Journal of Materials Chemistry C

Accepted Manuscript

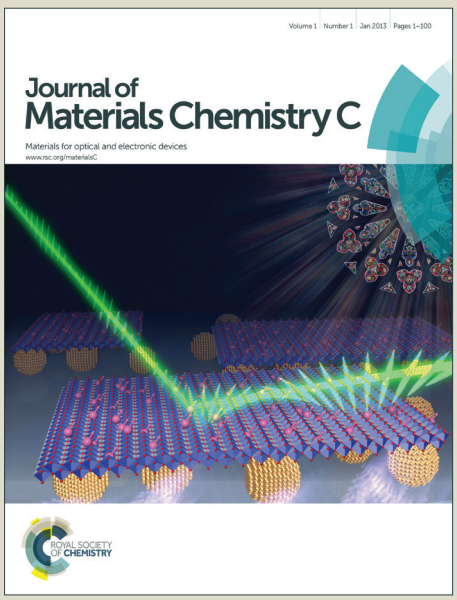

ROYAL SOCIETY OF CHEMISTRY

www.rsc.org/materialsC

Journal of Materials Chemistry C

RSC Publishing

ARTICLE

Improved performance of organic solar cells by incorporating silica-coated silver nanoparticles in buffer layer

Cite this: DOI: 10.1039/x0xx00000x

Received ooth January 2012,
Accepted ooth January 2012

DOI: 10.1039/x0xx00000x

www.rsc.org/

Yang Hao [a], Jingcheng Song,[a] Fan Yang,[a] Yuying Hao,[a]* Qinjun Sun,[a] Junjie Guo,[b,] Yanxia Cui,[a] Hua Wang,[c] Furong Zhu[d]*

Abstract: We demonstrate that the use of silica-coated silver nanoparticles in buffer layer allows improving the performance of organic solar cells. It is found that only large sized Ag nanoparticles have the advantages for increasing the electric field distribution in the active layer, thereby light absorption, caused by the localized surface plasmonic resonance and far-field scattering. Moreover, the scattering of silica-coated silver nanoparticles is a more important contributor to the light harvesting due to the existence of silica coating. It is also demonstrated that the silica coating is favorable to enhance exciton dissociation due to reducing the exciton quenching occurred at the interface between bare Ag nanoparticles and active layer. Besides, silica-coated silver nanoparticles also promote hole transport and extraction, which is presumably explained by introducing "dopant" levels within the band gap of the PEDOT:PSS and reducing hole trapping in bare silver surface. The combination of all these benefits results in a 25.4% improvement in photocurrent density and an increase of 19.2% in power conversion efficiency. This work indicates that the silica-coated silver nanoparticles as light trapping elements is more efficient than the bare silver nanoparticles in such a plasmonic organic solar cells. The systematical exploration on the optical and electrical effect of silica-coated silver nanoparticles contribute to a more comprehensive understanding on the mechanism of performance improvement of the plasmonic OSCs.

1. Introduction

Organic solar cell (OSCs) have great potential as a clean and renewable energy source technology due to solution-based fabrication process, light weight, transparency as well as their compatibility with large area flexible substrates.[1-3]At the present, power conversion efficiency (PCE) of OSCs is less satisfactory compared with their inorganic counterparts. One of the limitations is insufficient light absorption in the thin organic photoactive layers. Absorption enhancement in OSCs cannot be simply realized by using thicker active layer due to the mismatch between optical absorption length and charge transport scale, caused by the low carrier mobility in organic materials. Therefore, it is necessary to find ways to enhance light absorption effectively in the active layer without increasing its thickness. Different approaches have been reported including incorporating metal nanoparticles (NPs) and periodic surface plasmonic structures in OSCs to boost light absorption.[4-6]In metal NPs-incorporated OSCs, metal NPs function as sub-wavelength antenna, the increase of the absorption in the active layer is attributed to the enhanced electromagnetic field due to the excitation of localized surface plasmon resonance (LSPR).[5] On the other hand, metal NPs, serving as scattering centers, also increase the length of the optical path contributing to light absorption enhancement in solar cells.[5]

Up to date, the metal NPs with different materials, shapes, sizes have been introduced in various layers in OSCs.[7-22]The plasmonic OSCs seem attractive, but there exists significant challenges as well. There are some controversy reports, e.g., with favorable[10, 14, 17-18] and unfavorable [23-26] effects on the performance of OSCs. Although light absorption enhancement in metal NPs-based OSCs is observed, the bare metal NPs in active layer also induce charge recombination and exciton

quenching near the vicinity of metal surface due to dipole-dipole and charge-trapping coulpling.[27]Therefore the electrical losses due to undesired exciton quenching and charge-trapping offset the optical enhancement generated by metal NPs.[18] In order to avoid the exciton quenching and charge-trapping and maintain the advantage of metal NPs-induced absorption enhancement, the strategy of forming a thin dielectric layer coated metal NPs was proposed.[28] The solutions of placing the metal NPs outside active layer[7-13, 14-16, 19-21] are more effective for improving the absorption in the cells, thereby PCE, due to LSPR and/or far-field scattering of metal NPs. But Choy et al. suggested that the strong near field around Au NPs has limited contribution to light absorption enhancement in the active layer as LSPR effect mainly distributes laterally along anode/buffer layer interface. The improvement in PCE originates from the enlarged contact area between active layer and buffer layer and improved the conductivity of buffer layer.[29]

In this work, we incorporated the large size silica-coated Ag NPs (named as Ag@SiO_2NPs) in poly (3,4-ethylenedioxy-thiophene)–poly(styrenesulfonate) (PEDOT:PSS) buffer layer to improve the PCE. Indeed, Ag@SiO_2NPs incorporated in interface of active layer/buffer layer for improving PCE has been reported by other groups[30]. The difference with the existing work is that here Ag @SiO_2 NPs is incorporated within buffer layer and some large nanoparticles are able to protrude partly into active layer. This solution has advantages in improving PCE through: (1) increasing light absorption in active layer by inducing simultaneouly the far-field scattering effect and laterally distributed LSPR, caused by the large size Ag@SiO_2NPs; (2) reducing exciton quenching occurred at the interface between bare metal and active layer by coating Ag NPs using SiO_2 insulating thin layer and thus increasing exciton dissociation; (3) promoting hole transport and extraction by introducing "dopant" levels within the band gap of the PEDOT:PSS and reducing hole trapping in bare silver surface; and (4) such a positional way of Ag@SiO_2 less disturbing the morphology of the active layer, which is also a key factor for high PCE. The combination of all these benefits results in 25.4% improvement in photocurrent density and 19.2% in PCE as compared to the optimized control cell without NPs. Our results confirm that such a positional way of Ag@SiO_2 lead to a more excellent OSC than placing Ag@SiO_2NPs in the interface active layer/buffer layer, which was adopted in literature[30]. This work offers a more optimized design for the Ag@SiO_2 NPs integrated OSC. Additionally, we systematically explored the optical and electrical effect of Ag@SiO_2 NPs to contribute to a more comprehensive understanding on the mechanism of improvement of performance for the Ag@SiO_2 NPs integrated OSC.

2. Experimental

2.1. Synthesis of metal nanoparticles

The Ag and Ag@SiO_2NPs were synthesized using a simple and low-cost wet chemical method.[31-32]First, the ethylene glycol reduction agent is used to reduce the silver ions (Ag^+) in silver nitrate forming Ag NPs in the presence of poly (vinyl pyrrolidone) (PVP) at a high temperature. The size of Ag NPs can be tuned by controlling the amount of PVP and the reaction temperature. After reaction at 120-130℃ for 1 h, the Ag NPs were collected by centrifugation and washed sequentially by ethanol and water for several times. Next, the Ag NPs were then encapsulated with silica by the following way: the homogeneous Ag solution in ethanol was mixed with ammonium hydroxide under stirring, and then tetraethyl orthosilicate (TEOS) was slowly injected with continuous stirring. The reaction was continued for 6 h. The Ag@SiO_2 nanoparticles were separated by centrifugation and washed sequentially by ethanol and water for several times. The thickness of the silica coating layer increases gradually with increase of the TEOS doping ratio in the reaction.

2.2. Fabrication of OSCs

The Ag@SiO_2-incorporated OSCs have the device structure of glass/ITO/PEDOT:PSS:Ag@SiO_2NPs(30nm)/P3HT:PC_{60}BM (220nm)/LiF(1nm)/Al(150nm), as shown in Fig.1 (a). ITO-coated glass substrates were cleaned with acetone and isopropyl alcohol, and then treated by UV ozone. About 30nm-thick PEDOT:PSS layer with different Ag@SiO_2 doping ratios was spin-coated onto ITO at 3500 rpm for 60 s, and annealed at 120℃ for 30min in air. Next, a 220 nm active layer was spin-coated on PEDOT:PSS using the P3HT (9mg/ml) and PC_{60}BM (9mg/ml) blend solution in chlorobenzene at 600 rpm for 30 s. Finally, the devices were completed by deposition of a top electrode LiF (1nm)/Al (100nm), thermal evaporated in a vacuum with a base pressure of 5×10^{-4} Pa. A set of structurally identical control OSCs with and without Ag NPs were also fabricated for comparison studies. The cross-sectional view of control cells is shown in Figs.1(b) and 1(c).

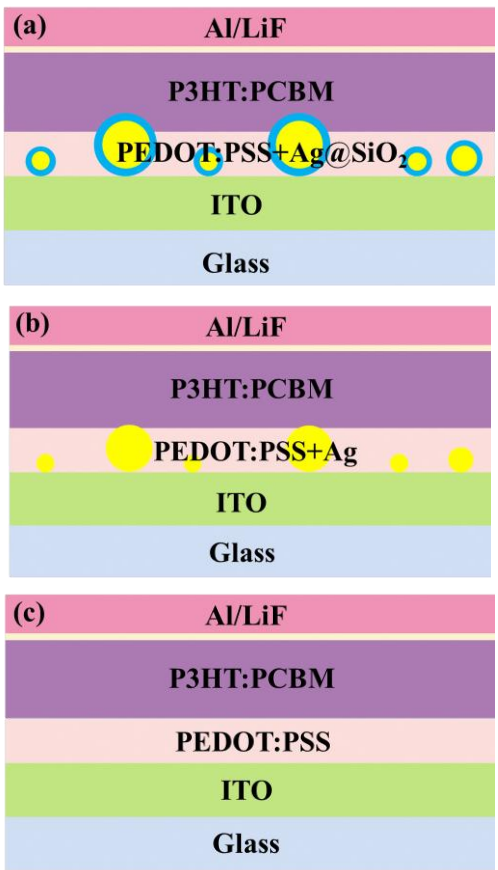

Fig.1 Cross-sectional view of different OSCs made with (a) Ag@SiO_2NPs and (b) Ag NPs along with (c) control cell without NPs.

2.3. Characterization

Scanning transmission electron microscope (STEM) images of the Ag NPs and Ag@SiO_2NPs were measured using a fifth-order aberration-corrected STEM (Nion-UltraSTEM100) with a cold field emission electron source. The absorption spectra of the pristine Ag NPs and Ag@SiO_2NPs in ethanol solution were measured using a HITACHI U-3900 UV-Visible Spectrophotometer at room temperature. And the absorption spectra of the multilayer film (MLF) of ITO/PEDOT:PSS /P3HT:PC_{60}BM with and without NPs in the PEDOT:PSS layer were also recorded by the same measurement system. Current density–voltage (J–V) characteristics of devices in dark and under illumination were measured using a programmable Keithley 2400 measurement source. The cells were illuminated using AM 1.5G solar simulator (ABET Technologies Sun 3000 Solar Simulator) with an irradiation intensity of 100 mW/cm^2, calibrated using a standard Si cell. External quantum efficiency (EQE) as a function of wavelength was recorded using ZOLIX CSC1011, where the light source is provided by an Ushio UXL-553Xenonshort arc lamp.

3. Results and discussion

STEM images of Ag NPs and Ag@SiO_2 NPs are shown in Figs.2(a) and 2(b). It is found that the size distribution of a majority of nanoparticles is over the diameter range from15 nm to 36nm, as shown in Fig. 2(a). But there exist some small sized nanoparticles that are in diameter range from 2 nm to 10nm in the samples. It is also clearly seen from Fig.1(b) that the Ag@SiO_2 nanoparticles are successfully synthesized. The silica shell with an average layer thickness from 6 to 8 nm is coated uniformly and completely on the surface of the individual Ag NPs. Fig. 2(c) shows that the UV−vis absorption spectra of Ag@SiO_2 NPs and Ag NPs dispersed in ethanol solution. The absorption peak of Ag NPs due to the localized surface plasmonic resonance (LSPR) is localized at 404nm, while that of Ag@SiO_2 nanoparticles is red shifted to 414 nm.

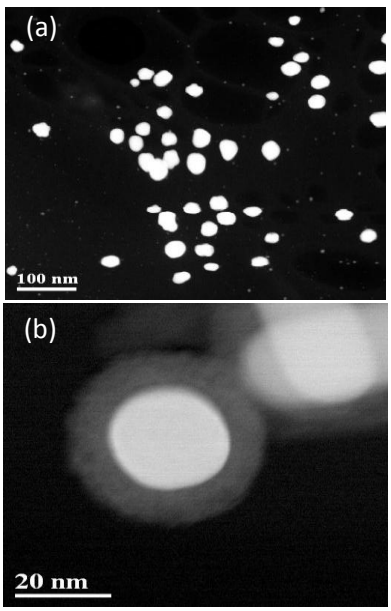

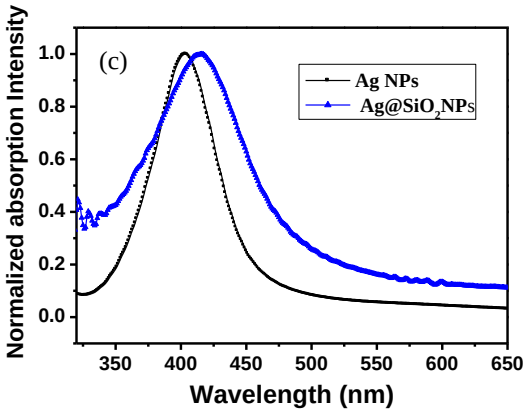

Fig. 2 (a) STEM images of Ag NPs with a diameter in the range from 15 nm to 36nm and (b) STEM images of Ag@SiO_2 NPs covered with a SiO_2 shell having an average layer thickness from 6 nm to 8nm; (c) Absorption spectra of Ag NPs and Ag@SiO_2 NPs in ethanol with LSPR peaks located at 404 nm and 414nm, respectively.

To investigate the effect of Ag@SiO_2 NPs on the photovoltaic performance of OSCs, devices made with and without Ag@SiO_2 NPs in the PEDOT:PSS layer were measured for comparison studies. Figs. 3(a) and 3(b) present J-V characteristics measured for OSCs made with different doping ratios of Ag@SiO_2NPs in PEDOT:PSS layer under illumination and in the dark.

Table 1 Performance parameters of OSCs with different doping ratio of Ag@SiO_2 NPs in PEDOT:PSS under AM 1.5G illumination at 100 mW cm^{-2}, and those of the optimized control cells with and without Ag NPs in PEDOT:PSS under the same condition.

Device	J_{sc} (mA/cm²)	V_{oc} (V)	*FF* (%)	PCE (%)	*Rs* (Ω cm²)	*Rsh* (Ω cm²)
Ag@SiO_2 1mg/ml	8.02	0.599	62.2	2.99	11.55	1063.08
Ag@SiO_2 2mg/ml	9.04	0.600	60.4	3.28	11.14	950.30
Ag@SiO_2 3mg/ml	9.67	0.594	58.3	3.35	10.31	806.28
Ag@SiO_2 4mg/ml	8.77	0.600	55.2	2.91	12.47	588.23
Ag NPs 2mg/ml	9.13	0.592	57.0	3.08	11.69	664.61
without NPs	7.71	0.600	60.9	2.81	12.65	1359.40

Performance parameters of OSCs made with different doping ratios of Ag@SiO_2 NPs in PEDOT:PSS, and the optimized control cells with and without incorporating Ag NPs are summarized in Table.1. The open circuit voltage (V_{OC}) remains almost a constant of about 0.6V for all devices. While the short circuit current density (J_{sc}) increases dramatically after incorporating Ag@SiO_2 NPs in the PEDOT:PSS layer. J_{sc} increases gradually with the doping ratio of Ag@SiO_2NPs increase from 0 to 3mg/ml, but begins to decrease as the doping ratio of Ag@SiO_2NPs increases to 4mg/ml. For 3mg/ml Ag@SiO_2 NPs, J_{sc} is increased to 9.67mA/cm^2 with 25.4% enhancement factor relative to the control cell without NPs. The existence of the optimal doping ratio is ascribed presumably to the transformation of incident light to thermal loss caused by the intrinsic absorption of Ag@SiO_2NPs, on the other hand, is associated with the disturbed transport and extraction of charge

carriers by Ag@SiO_2NPs, which will be discussed below. On the whole, the fill factor (*FF*) decreases with the increase in the doping ratio of Ag@SiO_2NPs. It has been well known that fill factor (*FF*) is associated with series and shunt resistances, which can be obtained from the inverse slope of illuminated *J*–*V* curves at short-circuit and open-circuit voltage, respectively[33]. The smaller series resistance (R_s) and larger shunt resistance (R_{sh}), the larger fill factor is. One can see from Table 1 that the series resistances are slightly reduced, while the shunt resistances are greatly decreased as the doping ratio of Ag@SiO_2NPs increases, as a result, leading to the decreased *FF*. But the enhancement of J_{sc} overwhelms the reduction of *FF* so that PCE of 3.35% with 19.2% enhancement factor was obtained for the optimized Ag@SiO_2NPs-integrated cell relative to the control cell without NPs. Fig. 3(b) presents *J*-*V* characteristics of the OSCs made with different doping ratios of Ag@SiO_2NPs in the dark. It can be seen from Fig.3(b) that the current rectification ratio of OSCs decreases and leakage current increases after incorporating Ag@SiO_2NPs. The highly elevated leakage current is consistent with the significant decrease of the shunt resistance of the Ag@SiO_2-integrated OSCs. Incorporating the Ag@SiO_2 NPs into the PEDOT:PSS buffer layer could induce some interface defects. Moreover, the small Ag NPs particles existing in sample could do not coated by SiO_2, which introduce the surface recombination centers. These defects and impurity result in the recombination current, which is responsible for the elevated leakage current density at the driving voltage of less than 0.5V and then the reduced shunt resistance.

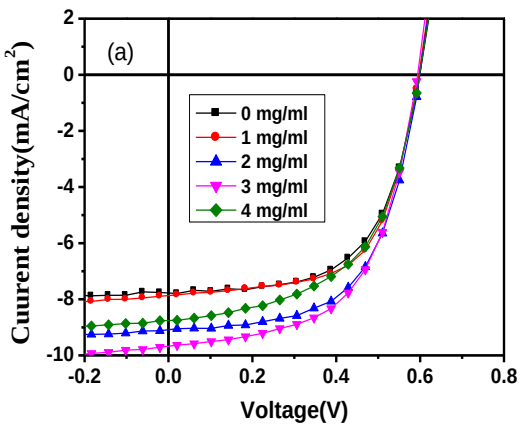

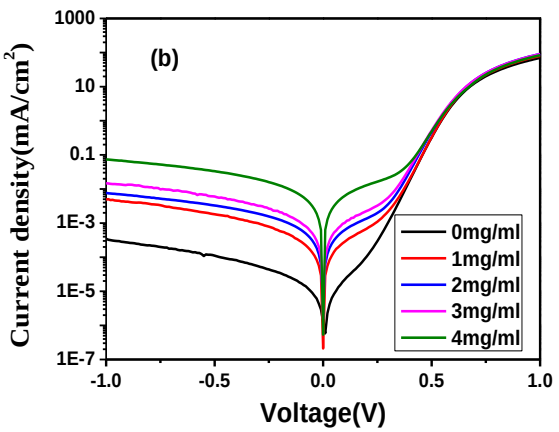

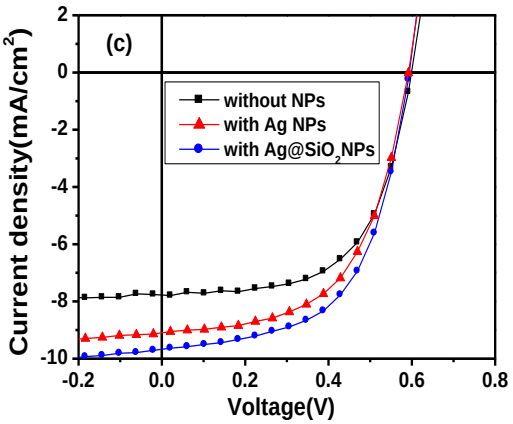

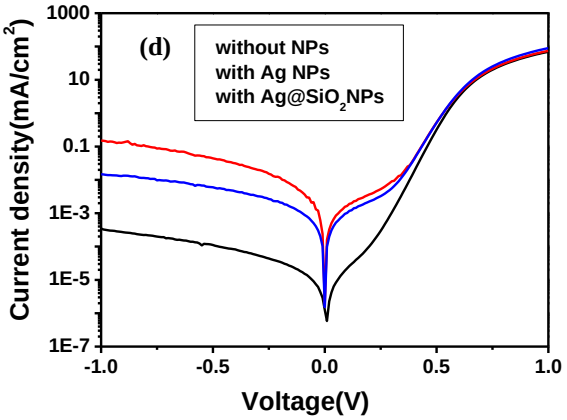

Fig.3 Current density-voltage characteristics measured for solar cells having different doping ratios of Ag@SiO_2 NPs in PEDOT:PSS layer under illumination (a) and (b) in dark. Current density-voltage characteristics of the optimized solar cells without and with NPs in PEDOT:PSS layer under illumination (c) and in dark (d), respectively.

As a comparison, Figs. 3(c) and (d) present *J*-V characteristics of the optimal OSCs with and without NPs under illumination and dark. J_{sc} of the optimized OSC with Ag@SiO_2 NPs is noticeably higher than that of the optimized control cells with Ag NPs. It is also found from Fig.3(d) that the Ag NPs integrated OSCs possess smaller shunt resistance and higher leakage current than that of the cells with Ag@SiO_2 NPs. This may be ascribed to the larger losing of charges due to recombination and trapping in bare metal surface.

To better elucidate the increment of J_{sc}, the EQE spectra of the optimized cells with and without NPs were measured, as shown in Fig. 4(a). It is observed that the larger enhancement in EQE is achieved by incorporating Ag@SiO_2NPs rather than Ag NPs, which is agreement with the change tendency of J_{sc}. EQE enhancement factor is calculated by subtracting the EQE of the cell without NPs from that of the cell with Ag@SiO_2NPs and then dividing by the EQE of the cell without NPs, as shown in inset of Fig. 4(a). A broad increase in EQE over a wavelength range from 300 to 700 nm is displayed for the Ag@SiO_2NPs integrated OSCs relative to the control cell without NPs.

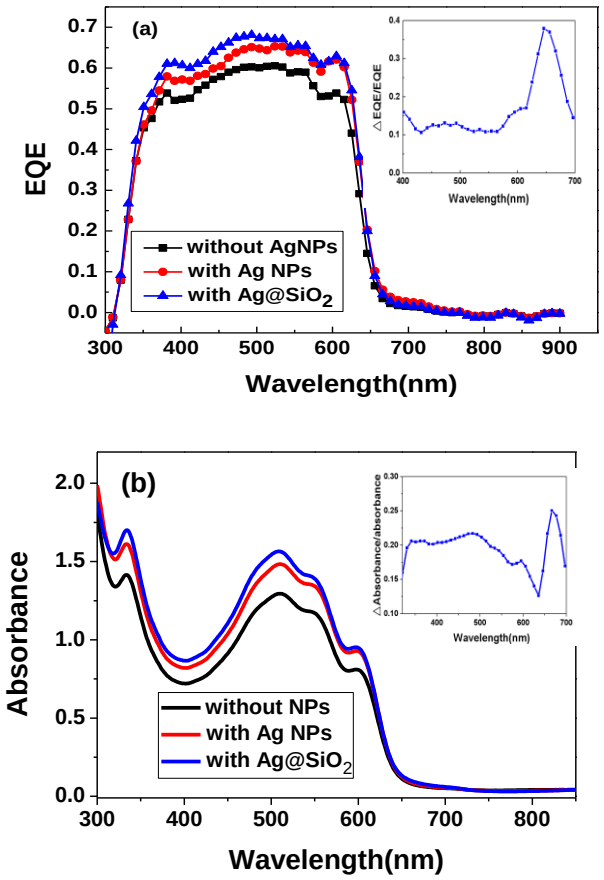

Fig.4 (a) EQE spectra of the optimized OSCs with and without NPs. Inset: EQE enhancement factor (b) UV−vis absorption spectra of the multilayer film of ITO/PEDOT:PSS/ P3HT:$PC_{60}BM$ without and with NPs in PEDOT:PSS. Inset: Absorption enhancement factor

To understand the enhancement in EQE, the optical effects of nanoparticles is investigated. The absorption spectra of multilayer film (MLF) of glass/ITO/PEDOT:PSS /P3HT:$PC_{60}BM$ with and without NPs in PEDOT:PSS were measured, as shown in Fig. 4(b). And absorption enhancement factor is achieved by subtracting the absorption spectrum of the MLF without NPs from that of the MLF with Ag@SiO_2NPs and then dividing by the absorption spectrum of the MLF without NPs, as shown in inset of Fig. 4(b). We found that the EQE enhancement is highly dependent on the absorption enhancement of active layer, but there also exists some mismatch between them. This means that EQE is also related with the electrical effect such as carrier transport and collection, except for the light-harvesting.

It is noted from inset of Fig. 4(b) that a broad increase in absorption of P3HT:$PC_{60}BM$ over a wavelength range from 300 to 700 nm is obtained by incorporating Ag@SiO_2 NPs into the MLF, which mismatch with that the narrow plasmonic resonance spectrum of Ag @SiO_2 NPs (see Figure 2c). We suggest that this inconsistent could originate from the far-field scattering effect of Ag @SiO_2 NPs. To confirm this hypothesis, the distributions of electric field |E| at 580nm under TM polarized light are investigated for the OSCs with Ag@SiO_2 NPs and Ag NPs in PEDOT:PSS using finite element method (FEM) in three–dimensional (3D) model respectively, as shown in Fig.5. The calculated device structure is completely same to the experimental device structure, where Ag NPs has the diameter of 36nm, while Ag@SiO_2NPs has 6nm-thick SiO_2 shell and core with diameter of 30nm or 15nm. Our numerical methods have been verified by studying the problems in Ref. 34. As shown in Fig. 5(a), the small size Ag@SiO_2NPs (15nm@6nm) incorporating into the PEDOT:PSS layer don't contribute to the absorption enhancement due to the lateral field distribution feature of the LSPR along the PEDOT:PSS layer, which is consistent with the results reported in Ref.29. However, when large size Ag@SiO_2NPs (30nm@6nm) are incorporated in the PEDOT:PSS layer, as illustrated in Fig. 5(b), the strong electric field round Ag@SiO_2NPs clearly penetrates into the active layer. But one can see from Fig. 6(c) that the plasmonic near-field around Ag NPs is far stronger than that around Ag@SiO_2NPs. It is well known that the transition probability of molecule from one ground state to the excited state is proportional to the square of electric field strength the molecule experiences, so it can be deduced that the introducing Ag NPs should leads to larger enhancement

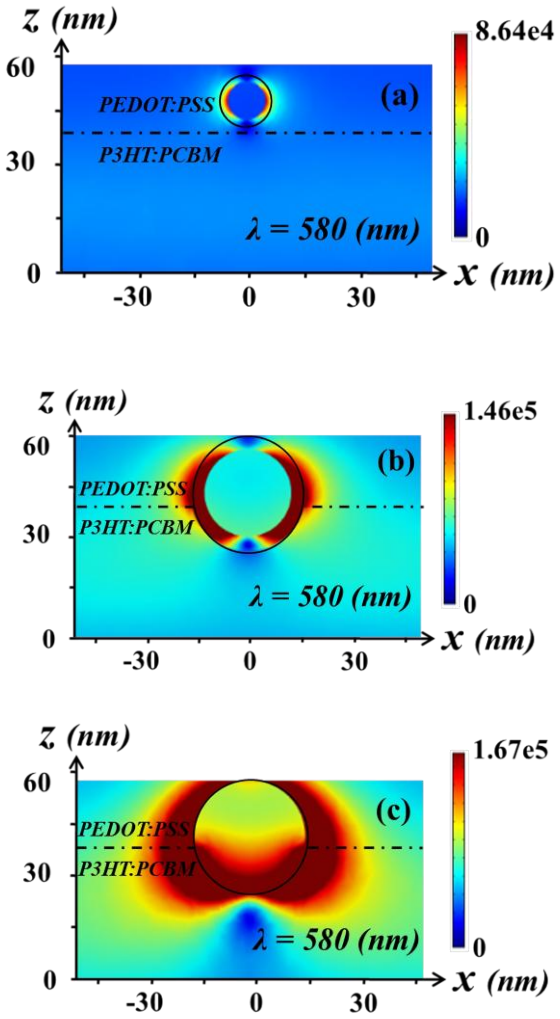

Fig.5 Distribution of electric field |E| at 580nm under TM polarized light for the OSC with small (a) and large (b) size Ag@SiO_2NPs along with Ag NPs (c) in PEDOT:PSS layer.

in light absorption of active layer. But the experimental resulting is reverse to theoretical analysis [see Fig. 4(b)]. Usually for metal nanoparticle, two factors contribute to the light absorption enhancement: first, local enhancement of the electromagnetic field in the vicinity of metal nanoparticle; alternatively, the scattering lengthening the optical path in the active layer. The above inconsistency means that Ag@SiO_2 NPs induces much stronger far-field scattering due to the presence of SiO_2 shell. Moreover, the scattering of Ag NPs@SiO_2 should be a more important contributor to the light harvesting than the plamonic near-field enhancement.

In order to further explore the effects of nanoparticles, we determine the maximum exciton generation rates (G_{max}) for the optimized OSCs with and without NPs. The current density-voltage characteristics of the optimized OSCs without and with NPs were measured under illumination and in dark when the devices were biased sweeping from +1 to -10 V. Following the analytical approach reported by Jyh-Lih Wu and co-workers[35], the dependence of the photocurrent density (J_{ph}) on the effective voltage (V_{eff}) is revealed, as shown in Fig. 6. The values of J_{ph} and V_{eff} are determined using the equations $J_{ph}=J_L-J_D$ and $V_{eff}=V_o-V_a$, respectively, where J_L and J_D are the current densities under illumination and in the dark respectively, V_o is the voltage when J_{ph} equals zero and V_a is the applied voltage. It can be seen from Fig. 6(a) that the value of J_{ph} reaches a saturated level at a sufficiently high V_{eff}. We therefore determined the values of the saturation photocurrent density (J_{sat}) and then calculate G_{max} by the equation $J_{sat} = qG_{max}L$, where q is the electronic charge and L is the thickness of the active layer, as shown in Table 2. One can see that incorporating Ag@SiO_2 NPs lead to the largest G_{max}. The enhanced G_{max} is associated with the increased light absorption, which is consistent with the absorption spectra characteristic of the MLF

Based on the maximum exciton generation rates (G_{max}), we calculated the exciton dissociation probabilities [P (E, T)], which are related to the electric field (E) and temperature (T), for the optimized OSCs with and without NPs. For OSCs, when the excitons are photogenerated, only a portion of them can be dissociated into free carriers. J_{ph} can be expressed using the equation $J_{ph} = qG_{max}P(E, T)L$. As a result, the value of P (E, T) at any bias can be obtained from the plot of the normalized photocurrent density (J_{ph}/J_{sat}) with respect to V_{eff}. Under the short-circuit conditions (V_a = 0 V), we obtained that $P(E,T)$ is 76%, 80% and 85% for the OSCs without and with AgNPs along with Ag@SiO_2 NPs, respectively. We found exciton dissociation probability is higher for the Ag @SiO_2 NPs integrated OSC. This means that the exciton quenching occurred at the interface between bare Ag NPs and active layer is reduced by coating SiO_2 insulating layer. The enhanced charge separation also contributes to the enhanced EQE and then J_{sc} except for the increased light absorption.

To further clarify the electrical effects of nanoparticles, we investigate the current-voltage characteristics of hole-only device of ITO/PEDOT:PSS (100nm)/MoO_3(5nm)/Ag without and with Ag@SiO_2NPs in PEDOT:PSS by adjusting the doping ratio of Ag@SiO_2NPs. The results indicate that the current-density of hole-only device first increases and then reduces with increasing the doping ratio of Ag@SiO_2 NPs at the same voltage, as shown in Fig. 7(a), which is consistent to the change trend of series resistance. This means that the electrical performance of PEDOT:PSS can be improved by incorporating appropriate amount of Ag@SiO_2 NPs. The improved electrical performance is presumably attributed to the introduction of "dopant" levels[36] within the band gap of the PEDOT:PSS by introducing Ag@SiO_2NPs, which could increase

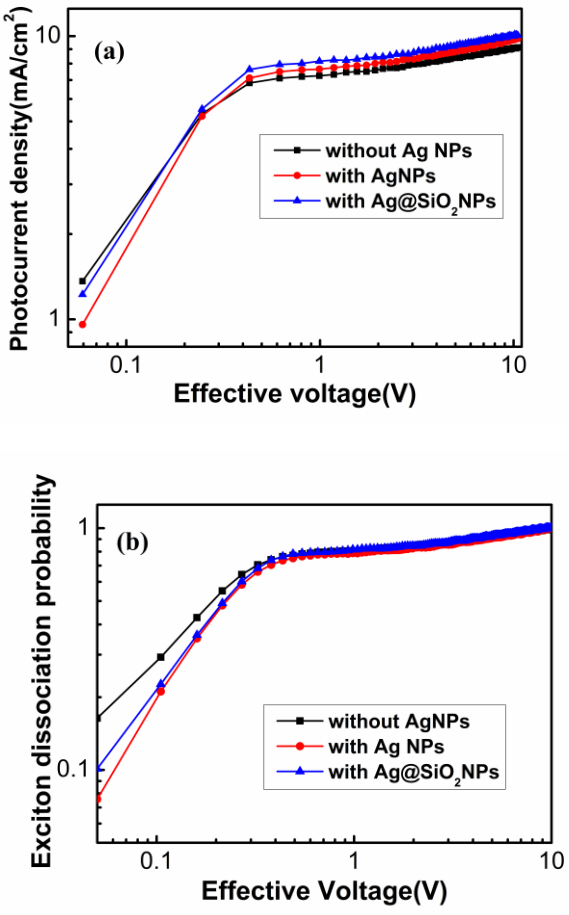

Fig.6 (a) Photocurrent density (J_{ph}) with respect to effective bias (V_{eff}) and (b) Exciton dissociation probability [$P(E,T)$] with respect to effective bias (V_{eff}) for the optimized OSCs with and without NPs

the hole transport and reduce the energy barrier of hole injection from ITO to PEDOT:PSS. But for too large doping ratio, the contact possibility between Ag@SiO_2 and ITO is increased, which lead to the enhanced contact resistance and thus inhibiting the hole injection. In order to confirm this concept, we investigated the current-voltage characteristics of hole-only devices of ITO/Ag@SiO_2 NPs /PEDOT:PSS (100nm)/MoO_3(5nm)/Ag, as shown in Fig.7(b), where Ag@SiO_2NPs are located at ITO/ PEDOT:PSS interface by spin-coating the ethanol solution of Ag@SiO_2NPs with different concentration of 2, 6 and 10mg/ml. One can see that the conductivity of the hole-only devices is first increased and then decreased as increasing the amount of Ag@SiO_2NPs at the ITO/PEDOT:PSS interface. This means that appropriate amount of Ag@SiO_2NPs were inserted at ITO/PEDOT:PSS interface to promote hole injection or extraction. But too large amount of Ag@SiO_2 NPs at ITO/PEDOT:PSS interface inhibits hole injection or extraction due to too large contract area between ITO and SiO_2.

We also compared the current-voltage characteristics of hole-only device of ITO/PEDOT:PSS(100nm) /MoO_3(5nm) /Ag with Ag NPs and Ag@SiO_2 NPs in PEDOT:PSS with the same doping ratio as the optimized OSCs, as shown in Fig.8. One can see that current-density of the hole-only device with Ag@SiO_2 NPs is higher at the

same voltage than that with Ag NPs. This means the conductivity of PEDOT:PSS is lower by introducing Ag NPs than Ag@SiO_2 NPs. The unexpected result could originate from the higher degree of charge loss due to surface recombination of bare metal.

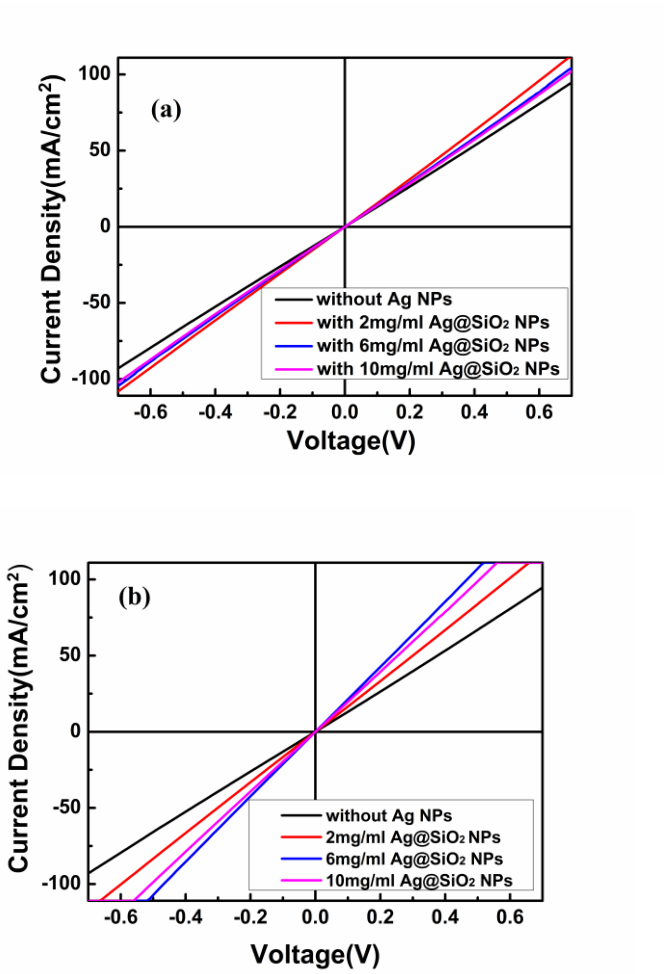

Fig. 7 (a) Current-voltage characteristics of hole-only device of ITO/PEDOT:PSS (100nm) /MoO_3 (5nm)/Ag without and with Ag@SiO_2 NPs in PEDOT:PSS in different doping ratio. (b) Current-voltage characteristics of hole-only device of ITO/Ag@SiO_2/ PEDOT:PSS (100nm) /MoO_3 (5nm)/Ag with different amount of Ag@SiO_2 NPs in ITO/ PEDOT:PSS interface.

In other word, SiO_2 shell could inhibit hole-trapping and reducing space charge accumulation and thus increasing hole transport.

Another electrical parameter, the ideality factor (n) of the optimized OSCs with and without NPs is derived from the *J–V* characteristics in the dark by using the relation[6]

$$\frac{\partial V}{\partial \ln I} = n\frac{KT}{q} + IR_s$$

Where q is the electronic charge, T is the absolute temperature, k is the Boltzmann constant and n is the ideality factor, Rs is series resistance. The n values were determined from y-axis intercept of the dV/dln$J$–J plot. The obtained values of n present Table 2. For an ideal diode the value of n is one, but experimentally obtained value of n are greater than unity. A departure from unity gives an indication of the imperfections in a diode. We found that the deviation degree of behaviour for the NP-integrated OSC is less than the control cell without NPs.

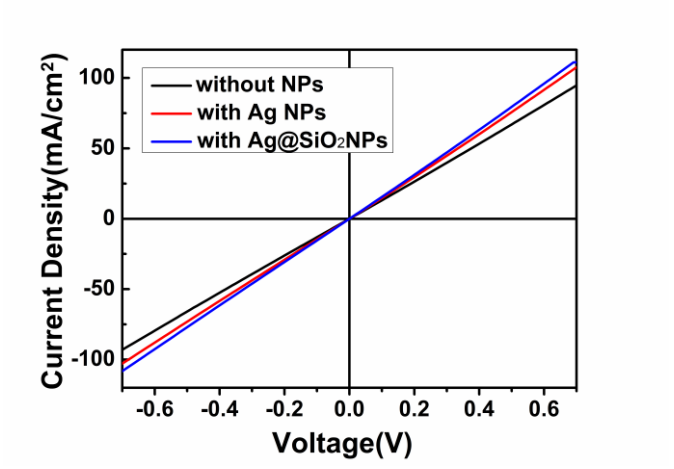

Fig.8 Current-voltage characteristics of hole-only device of ITO/PEDOT:PSS (100nm) /MoO_3 (5nm)/Ag without and with NPs in PEDOT:PSS with the same doping ratio as the optimized OSCs.

Table 2 Comparison of other parameters of the optimized OSCs with and without NPs

Device	J_{sat} (A m^{-2})	G_{max} (m^{-3} s^{-1})	P (E, T) (%)	Ideality factor (n)
without NPs	91	2.585×10^{27}	76	3.18
with Ag NPs 2mg/ml	97	2.755×10^{27}	80	2.07
with Ag@SiO_2 NPs 3mg/ml	105	2.982×10^{27}	85	2.17

Table 3 Comparison of the performance of OSCs with Ag @SiO_2 NPs incorporated in difference position, within buffer layer and at interface of buffer layer / active layer

OSCs with Ag@SiO_2 NPs	V_{oc} (V)	J_{sc} (mA/cm²)	FF (%)	PCE (%)	R_s (Ω cm²)	R_{sh} (Ω cm²)
at interface	0.592	9.47	60.0	3.28	9.45	533.72
within PEDOT:PSS	0.594	9.67	58.3	3.35	10.31	642.07

Finally, we compared the performance of OSCs with Ag @SiO_2 NPs incorporated in difference position including within buffer layer and at interface of buffer layer / active layer. The results confirm that the performance of OSCs with Ag @SiO_2 NPs in buffer layer is more excellent than in other position, as shown in Table 3, because such a positional way of Ag@SiO_2 NPs less disturb the morphology of the active layer than at interface of buffer layer / active layer, which is also a key factor for high PCE of OSCs.

4. Conclusions

In summary, we demonstrate that the performance of OSCs are improved by incorporating Ag@SiO_2NPs within the PEDOT:PSS layer. The short-circuit current increases from 7.71 mA/cm^2 for the optimized control cell without NPs to 9.67 mA/cm^2 for the optimized Ag@SiO_2NPs-integrated cells, with an enhancement factor of 25.4%. The current gain gives a rise of the conversion efficiency from η = 2.81% to 3.35%, with an enhancement factor of 19.2%. The enhancement is attributed to three factors: (1) the increased light absorption by the near-field enhancement effect and the far-field scattering of the large size

Ag@SiO_2NPs due to localized surface plasmon resonance, moreover the scattering is a more important contributor to the light harvesting; (2) the increased hole transport and extraction, which is presumably explained by introducing "dopant" levels within the band gap of the PEDOT:PSS and reducing hole trapping in bare silver surface; (3) the enhanced exciton dissociation due to the reduction of exciton quenching occurred at the interface between bare Ag NPs and active layer by SiO_2 coating. This work not only offers a more optimized design for the Ag@SiO_2 NPs integrated OSC, but also contribute to a more comprehensive understanding on the mechanism of improvement of performance.

Acknowledgements

This research work was financially supported by National Natural Science Foundation of China (61274056,11204205, 61205179, 21101111, 21071108,11204202, 91233208), Key Laboratory of Advanced Displays and System Applications, Ministry of Education, Shanghai University, International Science &Technology Cooperation Program of China (2012DFR50460), Shanxi Natural Science Foundation (2010021023-2, 2011021022-2,2012011020-4), New Teachers' Fund (20121402120017), Hong Kong Scholar Program(XJ2013002), and Talents for Early Career Scheme – Tertiary Education Division, Shanxi Province.

Notes and references

[a] Key Lab of Advanced Transducers and Intelligent Control System, Ministry of Education and Shanxi Province, College of Physics and Optoelectronics, Taiyuan University of Technology, Taiyuan 030024, China.

[b] Material Science and Technology Division, Oak Ridge National Laboratory, Oak Ridge, Tennessee 37831, USA

[c] Key Laboratory of Interface Science and Engineering in Advanced Materials, Taiyuan University of Technology, Taiyuan. Department of Physics and Institute of Advanced Materials,

[d]Hong Kong Baptist University, 224 Waterloo Road, Kowloon Tong, Hong Kong

*Corresponding author. E-mail address:haoyuyinghyy@sina.com, frzhu@hkbu.edu.hk

1 G. Li, R. Zhuand Y. Yang, *Nat. Photonics*, 2012, **6**, 153-161.

2 Z. He, C. Zhong, S. Su, M. Xu, H. Wu and Y. Cao, *Nat. Photonics*, 2012, **6**, 593-597.

3 G.M. Ng, G. M. Ng, E.L. Kietzke, T. Kietzke, L.W. Tan, P.K. Liew and F. R. Zhu, *Appl. Phys. Lett*. 90 (2007) 103505.

4 Q. Gan, F. J. Bartoli and Z. H. Kafafi, *Adv. Mater*, 2013, **25**, 2377-2377.

5 H. A. Aatwater and A. Polman, *Nat. Mater*, 2010,**9**, 205-213.

6 X.Z Wang, X.Z. Wang, J.W. Ho, Q. Y. Yang, H.L. Tam, G.X. Li, K.W. Cheah and F.R. Zhu, *Org. Electron*. 12 (2011) 1943.

7 S.S. Kim, S. I. Na, J. Jo, D.Y. Kim and Y.C. Nah, *Appl. Phys. Lett*, 2008, **93**, 073307.

8 A. J. Morfa, K. L. Rowlen, T. H. Reilly, M. J. Romero and J.V.D. Lagemaat, *Appl. Phys. Lett*, 2008,**92**, 013504.

9 N. Kalfagia，P.G. Karagiannidis, C. Pitsalidis, N.T. Panagiotopoulos, C. Gravalidis, S. Kassavetis, P. Patsalas and S. Logothetidis, *Sol. Energy Mater. Sol. Cells*, 2012, **104**, 165-174.

10 H. S. Noh, E. H. Cho, H. M. Kim, Y. D. Han and J. Joo, *Org. Electronics*, 2013, **14(1)**, 278-285.

11 K. Leonard, Y. Takahashi, J. You, H. Yonemura, J. Kurawaki and S. Yamada, *Chem. Phys. Lett*. 2013, **584,**130-134.

12 B. Wu, T. Z. Oo, X. Li, X. Liu, X. Wu, E. K. L. Yeow, H. J. Fan, N. Mathews and T. C. Sum, *J. Phys. Chem*. C 2012, **116**, 14820-14825.

13 X. Li , W. C. H. Choy , H. Lu , W. E. I. Sha and A. H. P. Ho, *Adv. Funct. Mater*. 2013, **23**, 2728-2735.

14 J. H. Lee , J. H. Park , J. S. Kim , D. Y. Lee and K. Cho, *Org. Electron*, 2009,**10**, 416-420.

15 F. C. Chen , J. L. Wu , C. L. Lee , Y. Hong , C. H. Kuo and M. H. Huang , *Appl. Phys. Lett*. 2009 , **95** , 013305.

16 D. H. Wang, D. Y. Kim, K. W. Choi, J. H. Seo, S. H. Im, J. H. Park, O. O. Parkand A. J. Heeger, *Angew. Chem*, 2011,**123**, 5633-5637.

17 Charlie C. D. Wang, Wallace C. H. Choy, C. Duan, Dixon D. S. Fung, Wei E. I. Sha, F.-X. Xie, F. Huang and Y. Cao, *J. Mater. Chem.*, 2012, **22**, 1206-1211.

18 J. L. Wu , F. C. Chen, Y. S. Hsiao, F. C. Chien, P. Chen, C. H. Kuo, M. H. Huang and C. S. Hus, *ACS Nano*, 2011, **5** , 959-967.

19 A. Kirkeminde, M. Retsch, Q. Wang, G. W. Xu, d R. Q. Hui, J. Wud and S. Q. Ren, *Nanoscale*, 2012, **4**, 4421.

20 L. Lu, Z. Luo, T. Xu and L. Yu, *Nano Lett*, 2013, **13**, 59−64.

21 L. Qiao, D. Wang, L. Zuo, Y. Ye, J. Qian, H. Chen, S. He, *Applied Energy*, 2011, **88**, 848-852.

22 V. Kochergin, L. Neely, C.-Y. Jao and H. D. Robinson, *Appl. Phys, Lett.* 2011, **98**, 133305

23 B. Wu, X. Y. Wu, C. Guan, K.F. Tai, E. K. L. Yeow, H. J. Fan, N. Mathews and T. C. Sum, *Nat. Communications*, 2013, **4:2004**, 1-7.

24 K. Topp, H. Borchert, F. Johnen, A. V. Tunc, M. Knipper, E. von Hauff, J. Parisiand K. Al-Shamery, *J. Phys. Chem. A*, 2010, **114**, 3981-3989.

25 W. J, Yoon, K.Y Jung, J. Liu, T. Duraisamy, R. Revur, F. L. Teixeira, S. Sengupta and P. R. Berger, *Sol. Energy Mater. Sol. Cells*, 2010, **94**, 128-132.

26 M. Xue, L. Li, B. J. T. d. Villers, H. Shen, J. Zhu, Z. Yu, A. Z. Stieg, Q. Pei, B. J. Schwartz and K. L. Wang, *Appl. Phys. Lett*, 2011, **98**, 253302.

27 M. Salvador, B. A. MacLeod, A. Hess, A. P. Kulkarni, K.Munechika, Jennifer I. L. Chen and D. S. Ginger, ACS Nano, 2012, 6(11),10024-10032

28 V. Jankovi, Y. (Michael) Yang, J. You, L. Dou, Y. Liu, P. Cheung, J. P. Chang, and Y. Yang, *ACS Nano*, 2013, **7(5)** 3815-3822

29 Dixon D. S. Fung, L. Qiao, Wallace C. H. Choy, C. Wang, Wei E. I. Sha, F. Xie and S. He, *J. Mater. Chem.*, 2011, **21(41)**, 16349-16356.

30 H. Choi, J.P. Lee, S.J. Ko, J.W. Jung, H. Park, S. Yoo, O. Park, J. R. Jeong, S. Park, and J. Y. Kim, *Nano Lett*, 2013, **13**, 2204−2208

31 F. Zhang, G.B. Braun, Y.F. Shi, Y.C. Zhang, X.H. Sun, N.O. Reich, D.Y. Zhao and G. Stucky, *J. Am. Chem. Soc.*, 2010, **132 (9)**, 2850–2851

32 J.P Yang, F. Zhang, Y.R. Chen, S. Qian, P. Hu, W. Li, Y.H. Deng, Y. Fang, L. Han, M. Luqmanb and D.Y. Zhao, *Chem. Commun.*, 2011, **47,** 11618-11620.

33 A. Moliton and J.-M. Nunzi, *Polym Int* 2006, **55**, 583-600

34 K. Islam, A. Alnuaimi, E. Battal, A. K.Okyay, A. Nayfeh, Solar Energy, 2014, **103**, 263–268

35 J.-L. Wu, F.-C. Chen, Y.-S. Hsiao, F.-C. Chien, P. Chen, C.-H. Kuo, M.H. Huang, and C.-S. Hsu, *ACS Nano*, 2011, **5(2)** 959-967.

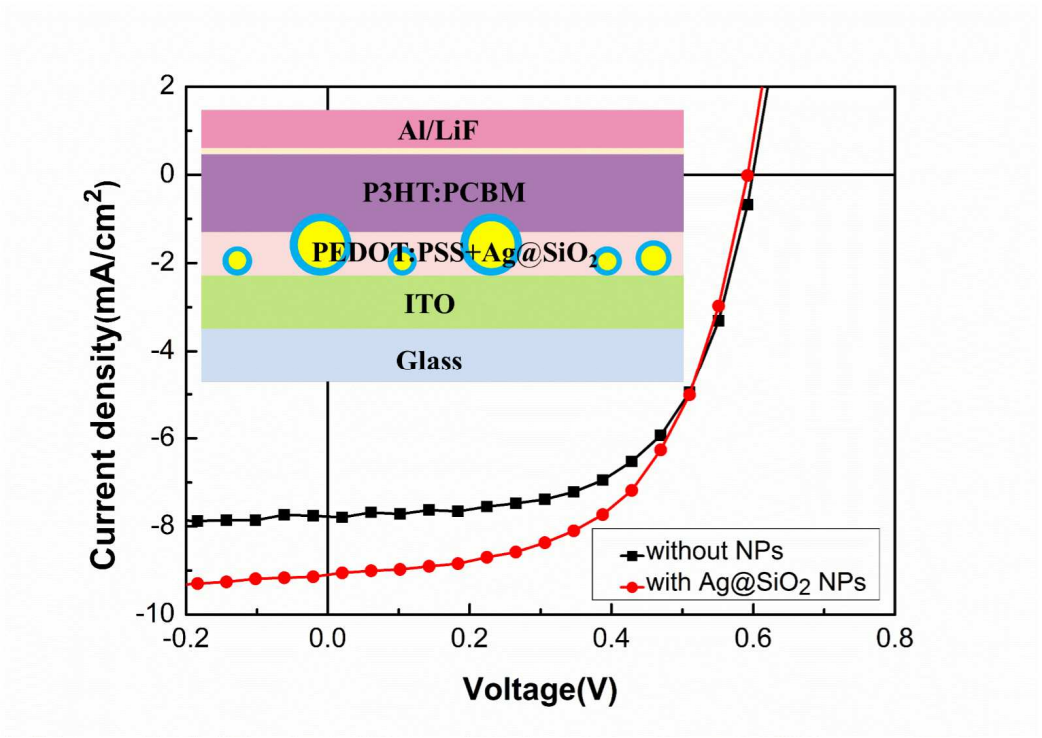

An enhancement of 19.2% in PCE is obtained by incorporating silica-coated silver nanoparticles into buffer layer of organic solar cells